

# Manipulation of Vortices by Localized Impurities in Bose-Einstein Condensates

M.C. Davis<sup>1</sup>, R Carretero-González<sup>1</sup>, Z. Shi<sup>2</sup>, K.J.H. Law<sup>2</sup>, P.G. Kevrekidis<sup>2</sup>, and B.P. Anderson<sup>3</sup>

<sup>1</sup>*Nonlinear Dynamical Systems Group\*, Department of Mathematics and Statistics,  
and Computational Science Research Center†, San Diego State University, San Diego CA, 92182-7720, USA.*

<sup>2</sup>*Department of Mathematics and Statistics, University of Massachusetts, Amherst MA 01003, USA*

<sup>3</sup>*College of Optical Sciences and Department of Physics,  
University of Arizona, Tucson AZ, 85721, USA.*

(Dated: October 30, 2018)

We consider the manipulation of Bose-Einstein condensate vortices by optical potentials generated by focused laser beams. It is shown that for appropriate choices of the laser strength and width it is possible to successfully transport vortices to various positions inside the trap confining the condensate atoms. Furthermore, the full bifurcation structure of possible stationary single-charge vortex solutions in a harmonic potential with this type of impurity is elucidated. The case when a moving vortex is captured by a stationary laser beam is also studied, as well as the possibility of dragging the vortex by means of periodic optical lattices.

## I. INTRODUCTION

Interactions between localized impurities, or pinning centers, and flux lines in type-II superconductors have long been of interest in condensed matter physics [1], with much recent work focusing on the pinning effects of arrays of impurities [2]. Similar studies of the interactions between a vortex array in a rotating Bose-Einstein condensate (BEC) and a co-rotating optical lattice [3] have further contributed to the interest in the physics of manipulating one array of topological structures with a second array of pinning sites. Depending on the configuration, depth, and rotation rate of the optical lattice, structural changes to the vortex array may be induced, and have now been experimentally observed [4]. Furthermore, combining an optical lattice with a rotating BEC may enable new investigations of other interesting phenomena, such as for example, alterations to the superfluid to Mott-insulator transition [5], production of vortex liquids with broken translational symmetry [6], and the existence of stable vortex molecules and multi-quantum vortices [7]. Yet despite these significant advances, the interactions between a *single* vortex and a single pinning site within a BEC, and the associated vortex dynamics, are not fully understood and many problems remain unexplored. A more complete understanding of such basic interactions may be important for the further development of many ideas and experiments regarding vortex pinning and manipulation, even for the case of vortex arrays. Here we undertake a theoretical and numerical study that examines the possibility of vortex capture and pinning at a localized impurity within the BEC, and the possibility of vortex manipulation and dragging by a moving impurity.

Manipulation of coherent nonlinear matter-wave structures [8, 9] in trapped BECs has indeed received some examination [10]. For example, in the case of nega-

tive scattering length (attractive) BECs in a quasi-one-dimensional (1D) scenario, numerical analysis shows that it is possible to pin bright solitons away from the center of harmonic trap. More importantly, pinned bright solitons may be adiabatically dragged and repositioned within the trap by slowly moving an external impurity generated by a focused laser beam [11]. Alternatively, bright solitons might be pinned and dragged by the effective local minima generated by adiabatically moving optical lattices and superlattices [12, 13]. The case of repulsive interactions has also drawn considerable attention. In the 1D setting, the effect of localized impurities on dark solitons was described in Ref. [14], by using direct perturbation theory [15], and later in Ref. [16], by the adiabatic perturbation theory for dark solitons [17]. Also, the effects and possible manipulation of dark solitons by optical lattices have been studied in Refs. [18, 19, 20].

In the present work, we limit our study of vortex-impurity interactions and vortex manipulation to the case of a positive scattering length (repulsive) pancake-shaped BEC that is harmonically trapped. We envision a single localized impurity created by the addition of a focused laser beam [8], which may in principle be tuned either above or below the atomic resonance, thereby creating a repulsive or attractive potential with blue or red detunings, respectively. We concentrate on the dynamics of a blue-detuned beam interacting with a single vortex.

Our manuscript is organized as follows. In the next section we describe the physical setup and its mathematical model. In Sec. III we study the static scenario of vortex pinning by the localized laser beam by describing in detail the full bifurcation structure of stationary vortex solutions and their stability as a function of the laser properties and the pinning position inside a harmonic trap. In Sec. IV we study vortex dragging by an adiabatically moving impurity. We briefly describe our observations also for the case of single vortex manipulation using an optical lattice, and touch upon the possibility of capturing a precessing vortex by a fixed impurity. Finally, in Sec. V we summarize our results and discuss some possible generalizations and open problems.

\*URL: <http://nlds.sdsu.edu/>

†URL: <http://www.csrc.sdsu.edu/>

## II. SETUP

In the context of BECs at nano-Kelvin temperatures, mean-field theory can be used to accurately approximate the behavior of matter-waves [8]. The resulting mathematical model is a particular form of the nonlinear Schrödinger equation (NLS) known as the Gross-Pitaevskii equation (GPE) [21, 22]. The GPE in its full dimensional form is as follows:

$$i\hbar\psi_t = -\frac{\hbar^2}{2m}\nabla^2\psi + g|\psi|^2\psi + V(x, y, z, t)\psi, \quad (1)$$

where  $\psi(x, y, z, t)$  is the wavefunction describing the condensate,  $m$  is the mass of the condensed atoms,  $g = 4\pi\hbar^2 a/m$  and  $a$  is their  $s$ -wave scattering length. The time-dependent external potential  $V(x, y, z, t)$  acting on the condensate is taken to be a combination of a static harmonic trap (HT) holding the condensed atoms, and a localized impurity (Imp) provided by a narrowly focused laser beam:

$$V(x, y, z, t) = V_{\text{HT}}(x, y, z) + V_{\text{Imp}}(x, y, z, t). \quad (2)$$

Herein we consider a harmonic trap potential

$$V_{\text{HT}}(x, y, z) = \frac{m}{2}\omega_r^2(x^2 + y^2) + \frac{m}{2}\omega_z^2 z^2, \quad (3)$$

with trapping frequencies  $\omega_r$  and  $\omega_z$  in the radial and  $z$  directions respectively. In general,  $V_{\text{Imp}}$  can be a negative or positive quantity, corresponding to an impurity that is an attractive or repulsive potential for the trapped atoms.

In the present study we further limit our attention to quasi-two-dimensional condensates, the so-called pancake-shaped condensates, by considering that  $\omega_z \gg \omega_r$  and that the tight ( $z$ ) direction condensate profile is described by the harmonic trap ground state in that direction [8, 9]. We also consider only cases where  $V_{\text{Imp}}$  is only a function of  $x$  and  $y$ , and possibly  $t$ , and hereafter remove the  $z$  dependence from our notation. Under this assumption it is possible to reduce the three-dimensional GPE (1) to an effective two-dimensional equation that has the same form as its three-dimensional counterpart but with  $g$  replaced by  $g_{2\text{D}} = g/\sqrt{2\pi}a_z$ , where  $a_z = \sqrt{\hbar/(m\omega_z)}$  is the transverse harmonic oscillator length [8, 9].

Furthermore, by measuring, respectively, two-dimensional density, length, time, and energy in units of  $\hbar\omega_z/g_{2\text{D}}$ ,  $a_z$ ,  $\omega_z^{-1}$ , and  $\hbar\omega_z$ , one obtains the standard form for the adimensionalized GPE in two dimensions:

$$iu_t = -\frac{1}{2}(u_{xx} + u_{yy}) + |u|^2u + V(x, y, t)u, \quad (4)$$

where the harmonic potential now reads

$$V_{\text{HT}}(x, y) = \frac{\Omega^2}{2}(x^2 + y^2), \quad (5)$$

and  $\Omega \equiv \omega_r/\omega_z$  is the adimensionalized harmonic trap strength. We use throughout this work a typical value

for the harmonic trap strength of  $\Omega = 0.065$  unless stated otherwise. Other harmonic trap strengths gave qualitatively similar results. In addition to the harmonic trap we impose a localized potential stemming from an external localized laser beam centered about  $(x_a(t), y_a(t))$  that in adimensional form reads

$$V_{\text{Imp}}(x, y, t) = V_{\text{Imp}}^{(0)} \exp\left(-\frac{[x - x_a(t)]^2 + [y - y_a(t)]^2}{\varepsilon^2}\right). \quad (6)$$

In this equation,  $V_{\text{Imp}}^{(0)}$  is proportional to the peak laser intensity divided by the detuning of the laser from the atomic resonance, and  $\varepsilon = w_0/\sqrt{2}$  where  $2w_0$  is the adimensional Gaussian beam width. A positive (negative)  $V_{\text{Imp}}^{(0)}$  corresponds to the intensity of a blue-(red-)detuned, repulsive (attractive) potential.

Steady-state solutions of the GPE are obtained by separating spatial and temporal dependencies as  $u(x, y, t) = \Psi(x, y) e^{-i\mu t}$ , where  $\Psi$  is the steady-state, time-independent amplitude of the wavefunction and  $\mu$  is its chemical potential (taken here as  $\mu = 1$  in adimensional units). Under the conditions that the location of the impurity is time-independent such that  $x_a$  and  $y_a$  are constant, this leads to the steady-state equation

$$\mu\Psi = -\frac{1}{2}(\Psi_{xx} + \Psi_{yy}) + |\Psi|^2\Psi + V(x, y)\Psi. \quad (7)$$

The initial condition used in this study was one that closely approximates a vortex solution of unit charge  $s = \pm 1$  centered at  $(x_0, y_0)$ :

$$\begin{aligned} \Psi(x, y) = & \Psi_{\text{TF}}(x, y) \tanh[(x - x_0)^2 + (y - y_0)^2] \\ & \times \exp\left[is \tan^{-1}\{(y - y_0)/(x - x_0)\}\right], \end{aligned} \quad (8)$$

where  $\Psi_{\text{TF}}(x, y) = \sqrt{\max(\mu - V(x, y), 0)}$  represents the shape of the Thomas-Fermi (TF) cloud formed in the presence of the relevant external potentials [8]. Subsequently, this approximate initial condition was allowed to converge to the numerically “exact” solutions by means of fixed point iterations.

## III. THE STATIC PICTURE: VORTEX PINNING AND THE BIFURCATIONS BENEATH

### A. Vortex Pinning by the Impurity

It is well-known that a vortex interacting with a harmonic trap undergoes a precession based upon the healing length of the vortex and the parameters which define the trap [23, 24, 25, 26, 27, 28, 29, 30]. Since we are introducing a localized impurity into the trap it is worthwhile to first observe the behavior of a vortex interacting with only the localized impurity, in the absence of the harmonic potential. We note that in this case, the parameters  $x_a$  and  $y_a$  may be neglected and the parameters  $x_0$  and  $y_0$  can be interpreted as the coordinates of the vortex relative to the impurity.

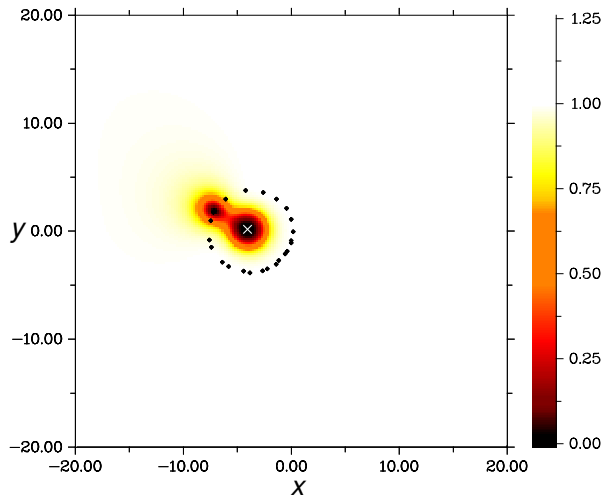


FIG. 1: (Color online) Density plot showing a snapshot of the interaction of the vortex with a localized impurity in the absence of the harmonic trap (i.e.,  $\Omega = 0$ ). The presence of the impurity (wider field depression) induces a clockwise rotation of the vortex (narrower field depression) along a path depicted by the dark dots. The parameters are as follows:  $(\mu, \Omega, s, V_{\text{imp}}^{(0)}, \varepsilon) = (1, 0, 1, 5, 1)$ . The colorbar shows the condensate density in adimensional units.

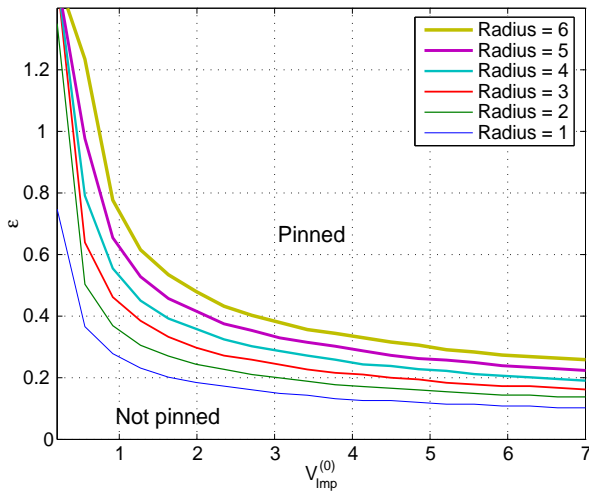


FIG. 2: (Color online) Phase diagram depicting the vortex pinning by the localized impurity of strength  $V_{\text{imp}}^{(0)}$  and width  $\varepsilon$ . Each curve represents a different pinning location at the indicated radii (i.e., distance from the center of the harmonic trap). Parameters are as follows:  $(\mu, \Omega, s) = (1, 0.065, 1)$ .

By symmetry, a vortex placed at the center of an impurity (i.e.,  $x_0 = y_0 = 0$ ) will result in a steady state without precession. However, a vortex placed off center with respect to the impurity will precess at constant speed around the impurity due to the gradient in the background field induced by the impurity [31]. In order to study this behavior in a simple physically meaningful setting we start with a positive-charge ( $s = 1$ ) vortex

without the impurity and then the impurity is adiabatically switched on at a prescribed distance away from the center of the vortex. We find that for  $V_{\text{imp}}^{(0)} > 0$  the vortex then begins to precess around the impurity in a clockwise direction. Reversing the sign of  $V_{\text{imp}}^{(0)}$  in order to create an attractive impurity induces a counter-clockwise precession with respect to the impurity. An example of the vortex precession induced by the impurity is shown in Fig. 1. It is crucial to note that if the impurity is turned on “close enough” to the steady-state vortex such that the impurity is within the vortex funnel then the vortex would begin its usual rotation but would be drawn into the center of the impurity, effectively pinning the vortex. This effective attraction is related to the emission of sound by the vortex when it is inside the funnel of the impurity as described in Ref. [32].

Throughout this work we follow the center of the vortices by detecting the extrema of the superfluid vorticity  $\omega$  defined as  $\omega = \nabla \times \mathbf{v}_s$  where the superfluid velocity in dimensional units is [8, 33]

$$\mathbf{v}_s = -\frac{i\hbar}{2m} \frac{\psi^* \nabla \psi - \psi \nabla \psi^*}{|\psi|^2}, \quad (9)$$

where  $(\cdot)^*$  stands for complex conjugation.

We now consider the net effect of the pinning induced by the impurity and the precession induced by the harmonic trap. Since one of our main goals is to find conditions needed for the manipulation of vortices using the repulsive impurity, a *minimum* requirement would be that the impurity’s pinning strength is sufficient to overcome the precession inside the trap and thus pin the vortex very close to the location of the impurity (i.e.,  $(x_0, y_0) \approx (x_a, y_a)$ ). Therefore, we seek to find the minimum conditions that an off-center vortex, at a particular radius measured from the center of the harmonic trap, could be pinned by a localized impurity at that same location. For certain combinations of beam parameters (strong beam intensity, or large beam widths), the vortex will remain localized near this point. For other parameters (weak intensity, small beam widths), the beam cannot overcome the vortex precession induced by the harmonic trap and the vortex would not remain localized near the beam position. This would give us a lower bound for the possible beam intensities and widths for which a vortex might be dragged to the corresponding position within the BEC. The existence of such pinned states was identified by searching in the impurity parameter space (strength  $V_{\text{imp}}^{(0)}$  and width  $\varepsilon$ ) for several off-center radii, i.e., distances measured from the center of the trap. The results are shown in the phase diagrams of Fig. 2 where each curve corresponding to a different radius (decreasing from top to bottom) depicts the boundary in  $(V_{\text{imp}}^{(0)}, \varepsilon)$  parameter space for which pinning is possible. In other words, for the points in parameter space below a given curve, one gets primarily vortex precession dynamics induced by the harmonic trap, whereas above these curves (i.e., for strong or wide enough impurities), the vortex is

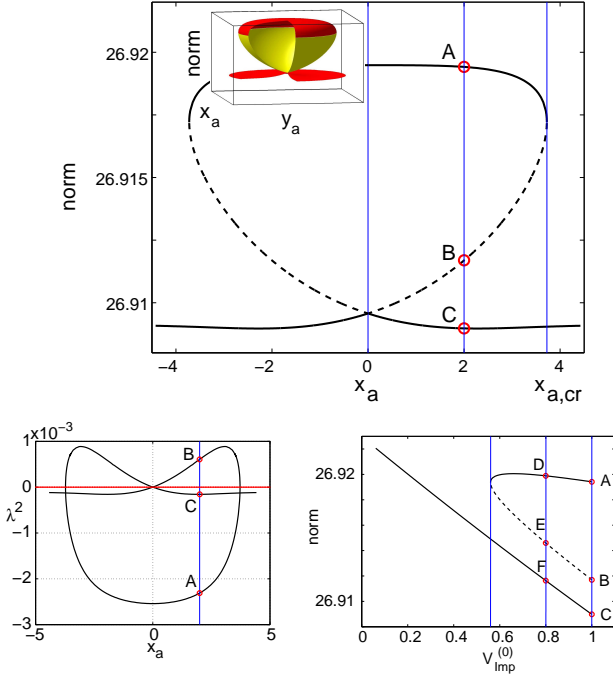


FIG. 3: (Color online) The top panel is a one-dimensional slice (for  $y_a = 0$ ) of the solution surfaces (represented in the inset panel) as a function of the position of the impurity ( $x_a, y_a$ ) for fixed  $V_{\text{imp}}^{(0)}$ . The vertical axis corresponds to the  $L^2$ -norm squared of the solution (i.e., the normalized number of atoms). The dashed lines (yellow (lighter) surface) correspond to unstable solutions, while the solid lines (red (darker) surfaces) correspond to stable solutions. The critical value of the radius,  $x_{a,\text{cr}} = 3.72$  as well as the characteristic value  $x_a = 2$  and  $x_a = 0$  are represented by vertical lines. The bottom left panel shows the squared bifurcating eigenvalues,  $\lambda^2$ , along these branches ( $\lambda^2 > 0$  corresponds to an instability), while the bottom right shows the saddle-node bifurcation as a function of  $V_{\text{imp}}^{(0)}$  for  $x_a = 2$  fixed (there are lines at  $V_{\text{imp}}^{(0)} = 0.57$ ,  $V_{\text{imp}}^{(0)} = 0.8$ , and  $V_{\text{imp}}^{(0)} = 1$ ). The solutions and spectra for each of the three branches, represented by circles (and letters) for each of the characteristic values of  $x_a$  and  $V_{\text{imp}}^{(0)}$  are presented in Fig. 4. For these branches  $(\mu, s, \varepsilon) = (1, 1, 0.5)$ .

trapped by the impurity and stays very close to it.

### B. Steady-state bifurcation structure

In this section we elaborate our investigation of the pinning statics and the associated dynamical stability picture. In particular, we thoroughly analyze the bifurcation structure of the steady states with single-charge vorticity in the setting investigated above (i.e. solutions to Eq. (7)) including their stability. The latter will be examined by the eigenvalues of the linearization around the steady state. Upon obtaining a steady state solution  $\Psi$  of Eq. (7) and considering a separable complex valued perturbation  $\tilde{u} = a(x, y)e^{\lambda t} + b^*(x, y)e^{\lambda^* t}$  of the steady state, we arrive at the following eigenvalue problem for

the growth rate,  $\lambda$ , of the perturbation:

$$\begin{pmatrix} \mathcal{L}_1 & \mathcal{L}_2 \\ -\mathcal{L}_2^* & -\mathcal{L}_1^* \end{pmatrix} \begin{pmatrix} a \\ b \end{pmatrix} = i\lambda \begin{pmatrix} a \\ b \end{pmatrix},$$

where

$$\begin{aligned} \mathcal{L}_1 &= -\mu - \frac{1}{2}(\partial_x^2 + \partial_y^2) + V + 2|\Psi|^2 \\ \mathcal{L}_2 &= \Psi^2. \end{aligned}$$

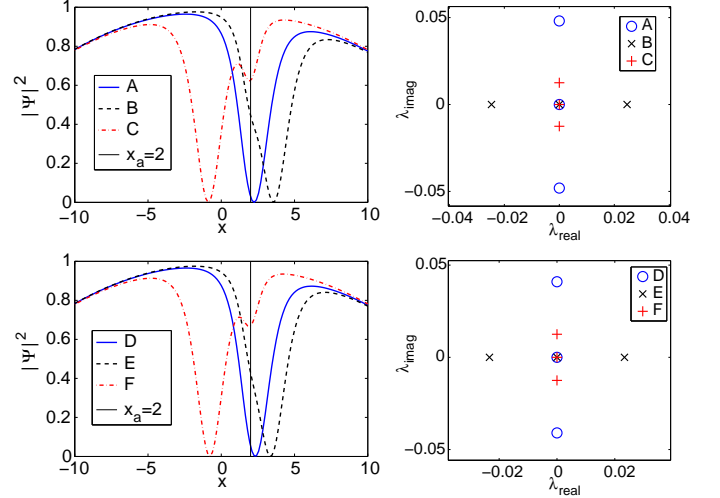


FIG. 4: (Color online) The solutions (left, zoomed in to the region where the vortices live) and corresponding linearization spectra in a neighborhood of the origin (right), for the various parameter values indicated by the circles in Fig. 3. The top (bottom) row corresponds to  $V_{\text{imp}}^{(0)} = 1$  ( $V_{\text{imp}}^{(0)} = 0.8$ ).

As evidenced by the bifurcation diagrams presented in Fig. 3, there exist three solutions (i.e., steady-state vortex positions) for any impurity displacement radius in the interval  $(0, x_{a,\text{cr}})$ , letting  $y_a = 0$  without any loss of generality. At the low end of the interval (i.e., for an impurity at the center of the trap,  $(x_a, y_a) = (0, 0)$ ) there is a transcritical bifurcation where the left (i.e., ones for negative  $x_a$ ) and right (i.e., for positive  $x_a$ ) solutions collide (see below for further explanation) and exchange stability. At the other end of the interval (i.e., for an impurity at  $(x_a, y_a) = (x_{a,\text{cr}}, 0)$ ) there exists a saddle-node bifurcation where two new steady-state vortex solutions can be thought of as emerging as  $x_a$  decreases to values  $x_a < x_{a,\text{cr}}$ , or conversely can be thought of as disappearing as  $x_a$  increases to values  $x_a > x_{a,\text{cr}}$ . Among them, one stable vortex position is found very close to the impurity (see cases “A” and “D” in Figs. 3 and Fig. 4), and another unstable vortex position further away from the trap center (see cases “B” and “E”) in Figs. 3 and Fig. 4). Considering only  $x_a$ , with  $y_a = 0$ , two solution branches are stable: one with the vortex sitting very close to the impurity (see cases “A” and “D” in Figs. 3 and Fig. 4),

and one with the vortex close to the center of the harmonic trap (see cases “C” and “F” in Figs. 3 and Fig. 4). The other solution is unstable (see cases “B” and “E” in Figs. 3 and Fig. 4), with the vortex sitting in the small effective potential minimum on the side of the impurity opposite the center of the harmonic trap. This branch of solutions collides with the one that has a vortex pinned at the impurity and the two disappear in a saddle-node bifurcation as the attraction of the impurity becomes too weak to “hold” the vortex (this bifurcation corresponds to the curves of critical parameter values in Fig. 2). At  $x_a = 0$ , the potential becomes radially symmetric and the solution with the vortex on the outside of the impurity becomes identical (up to rotation) to the one close to the origin. Indeed, at this point there is a single one-parameter family of invariant solutions with the vortex equidistant from the origin (i.e., for any angle in polar coordinates), in addition to the single solution with the vortex centered at  $(0,0)$ . The solutions in this invariant family, not being radially symmetric and being in a radially symmetric trap, necessarily have an additional pair of zero eigenvalues in the linearization spectrum to account for the additional invariance, i.e. they have 4 instead of 2 zero eigenvalues (note that the solution with the vortex in the center for  $x_a = 0$  only has a single pair of zero eigenvalues due to its radial symmetry). For  $x_a < 0$  the branches exchange roles (transcritical bifurcation) as the previously imaginary pair of eigenvalues for the stable  $x_a > 0$  branch (see cases “C” and “F” in Figs. 3 and Fig. 4) emerges on the real axis and the pair of previously real eigenvalues from the unstable  $x_a > 0$  branch (see cases “B” and “E” in Figs. 3 and Fig. 4) emerges on the imaginary axis, i.e. the branches exchange their stability properties, becoming the reflected versions of one another; see the bottom left panel of Fig. 3 and the right column of Fig. 4. In summary, for an impurity that is strong enough and close enough to the trap center (specifically,  $0 \leq x_a < x_{a,\text{cr}}$ , where  $x_{a,\text{cr}}$  depends of the strength of the impurity) it is possible to *stably* pin the vortex very close to the impurity. However, if the impurity is too far away from the trap’s center (specifically,  $x_a > x_{a,\text{cr}}$ ) the vortex can no longer be pinned by the impurity. The top image of Fig. 3 depicts the bifurcations via the  $L^2$ -norm squared (i.e., the normalized number of atoms) of the solution as a function of the radius,  $x_a$  (for  $y_a = 0$ ), and as a function of arbitrary impurity location  $(x_a, y_a)$  (inset).

In fact, the above picture holds for any fixed, sufficiently large  $V_{\text{imp}}^{(0)}$ . Conversely, the same bifurcation structure can be represented by a continuation in the amplitude of the impurity,  $V_{\text{imp}}^{(0)}$  (see bottom right panel of Fig. 3). In particular, for a fixed radius of  $x_a = 2$ , a continuation was performed and a saddle-node bifurcation appears for  $V_{\text{imp}}^{(0,\text{cr})} \approx 0.57$  where an unstable and a stable branch emerge (corresponding exactly to those presented in the continuation in  $x_a$ ). One can then infer that the critical  $V_{\text{imp}}^{(0)}$  decreases as  $x_a$  decreases.

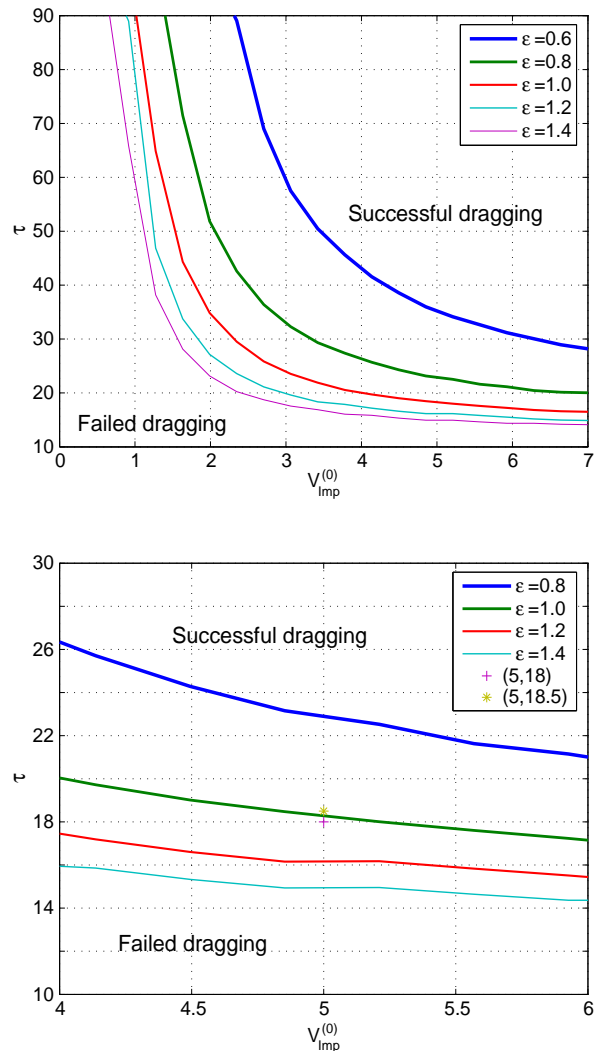


FIG. 5: (Color online) Parameter regions for successful manipulation of a single vortex inside a harmonic trap. The area above each curve corresponds to the successful dragging region. The bottom panel depicts a zoomed region of the top panel where the asterisk and cross correspond, respectively, to the manipulation success and failure depicted in Fig. 6. These panels indicate that higher intensity beams, and broader beams, can successfully drag vortices over shorter timescales than weaker, narrower beams.

#### IV. THE DYNAMICAL PICTURE: DRAGGING AND CAPTURING

##### A. Vortex Dragging

We would like now to take a pinned vortex and adiabatically drag it with the impurity in a manner akin to what has been proposed for bright [11, 12, 13] and dark solitons [18, 19, 20] in the quasi-1D configuration. Manipulation of the vortex begins with the focused laser beam at the center of the vortex. The laser is then adi-

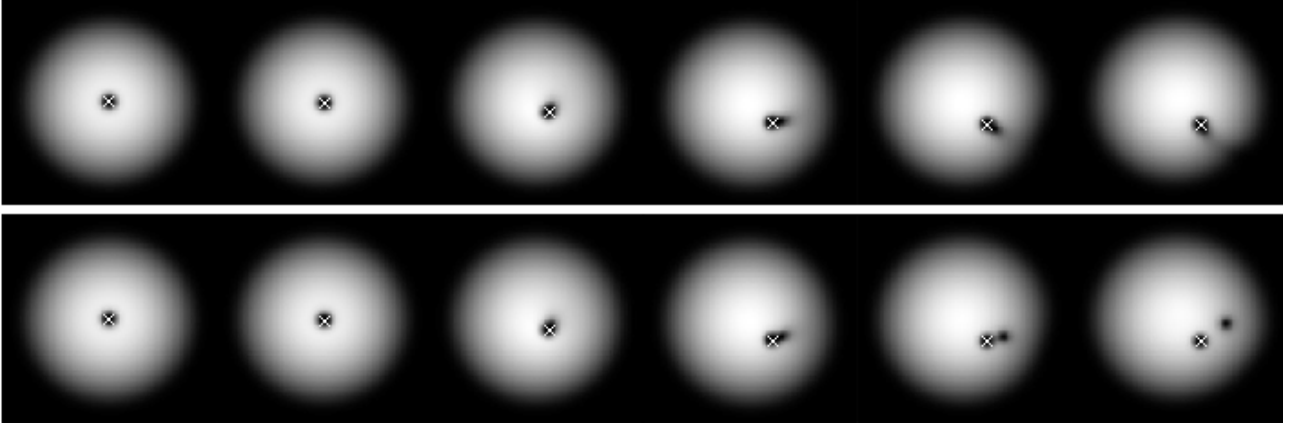


FIG. 6: Successful (top row) and failed (bottom row) vortex dragging cases by a moving laser impurity corresponding to the parameters depicted, respectively, by an asterisk and a cross in the bottom panel of Fig. 5. In both cases, the laser impurity, marked by a cross, with  $(V_{\text{Imp}}^{(0)}, \epsilon) = (5, 1)$  is moved adiabatically from  $(0, 0)$  to  $(5.43, -5.43)$  and the snapshots of the density are shown every  $0.5t^*$ . The top row corresponds to a successful manipulation for  $\tau = 18.5$  while the bottom row depicts a failed dragging for a slightly lower adiabaticity of  $\tau = 18$ .

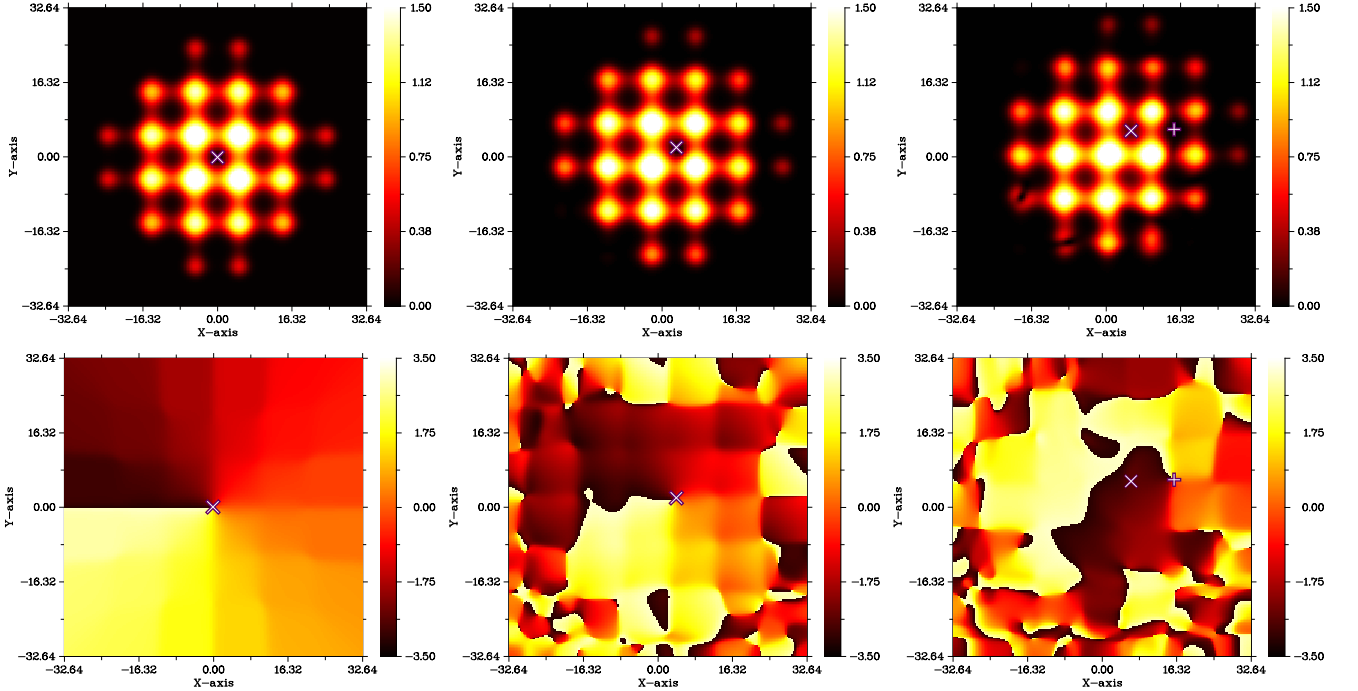


FIG. 7: (Color online) Vortex dragging by an optical lattice potential as in Eq. (12). The central high-intensity maximum of the optical lattice (depicted by a cross in the panels) is moved adiabatically from the initial position  $(x_a(0), y_a(0)) = (0, 0)$  to the final position  $(5.43, 5.43)$ . The top row depicts the BEC density (the colorbar shows the density in adimensional units) while the bottom row depicts the phase of the condensate where the vortex position (“plus” symbol in the right column) can be clearly inferred from the  $2\pi$  phase jump around its core. Observe how the vortex loses its guiding well and jumps to a neighboring well in the right column. The left, middle and right columns correspond, respectively, to times  $t = 0$ ,  $t = 0.5t^*$  and  $t = 2.5t^*$ . The remaining parameters are as follows:  $(V_0, k, \tau, \theta_x, \theta_y) = (1.4, 0.3215, 20, 0, 0)$ .

adiabatically moved to a desired location while continually tracking the position of the vortex. Adiabaticity for the motion of the impurity is controlled by the adiabaticity parameter  $\tau$  controlling the acceleration of the center

$(x_a(t), y_a(t))$  of the impurity as:

$$\begin{aligned} x_a(t) &= x_i - \frac{1}{2}(x_i - x_f) \left( 1 + \tanh \left[ \frac{t - t^*}{\tau} \right] \right), \\ y_a(t) &= y_i - \frac{1}{2}(y_i - y_f) \left( 1 + \tanh \left[ \frac{t - t^*}{\tau} \right] \right), \end{aligned} \quad (10)$$

where the initial and final positions of the impurity are, respectively,  $(x_i, y_i)$  and  $(x_f, y_f)$ . We will assume  $y_a(t) = 0$  (i.e.,  $y_i = y_f = 0$ ) for the discussion below. The instant of maximum acceleration is

$$t^* = \tanh^{-1} \left( \sqrt{1 - \delta\tau} \right) \tau, \quad (11)$$

where  $\delta$  is a small parameter,  $\delta = 0.001$ , such that the initial velocity of the impurity is negligible and that  $x_a(0) \approx x_i$  and  $x_a(2t^*) \approx x_f$  (and the same for  $y$ ). This condition on  $t^*$  allows for the reduction of parameters and allows us to ensure that we begin with a localized impurity very close to the center of the trap [i.e.,  $(x_a(0), y_a(0)) \approx (0, 0)$ ] and that we will drag it adiabatically to  $(x_f, y_f)$  during the time interval  $[0, 2t^*]$ . The next objective is to determine the relation between adiabaticity and the various parameters such as strength ( $V_{\text{Imp}}^{(0)}$ ) or the width ( $\varepsilon$ ) of the impurity in order to successfully drag a vortex outward to a specific distance from the center of the harmonic trap. In our study we set this distance to be half of the radius of the cloud (half of the Thomas-Fermi radius). We use the value  $t^*$  to also define when to stop dynamically evolving our system. In particular, we opt to continue monitoring the system's evolution until  $t_f = 3t^*$ . This choice ensures that a vortex that might have been lingering close to the impurity at earlier times would have either been “swallowed up” by the impurity and remain pinned for later times, or will have drifted further away due to the precession induced by the trap.

Applying this technique, along with a bisection method (successively dividing the parameter step in half and changing the sign of the parameter stepping once the threshold pinning value is reached) within the span of relevant parameters yields the phase diagram depicted in Fig. 5. The various curves in the figure represent the parameter boundaries for successful dragging of the vortices for different impurity widths (increasing widths from top to bottom). All the curves for different widths are qualitatively similar corresponding to higher values of the adiabaticity parameter as the width is decreased. This trend continues as  $\varepsilon$  approaches the existence threshold established in Fig. 2. In Fig. 6 we depict snapshots for the two cases depicted by an asterisk (successful dragging) and a cross (failed dragging) in the lower panel of Fig. 5.

All of the numerical simulations discussed above deal with dragging the vortex by means of the localized impurity. As with previous works of vortex manipulations we also attempted to produce similar results via an optical lattice (OL) potential generated by counter-propagating laser beams [8]. In one dimension, the case of bright solitons manipulated by OLs has been studied in Refs. [12, 13] while the dark soliton case has been treated in Refs. [18, 19, 20]. For a 1D OL, simply described by  $V_{\text{OL}}^{1D}(x) = V_0 \cos^2(kx + \theta_x)$  where  $k_x$  and  $\theta_x$  are the wavenumber and phase of the OL, the potential minima (or maxima) are isolated from each other providing good effective potential minima for pinning and

dragging. On the other hand, when expanded to 2D, the OL reads:

$$V_{\text{OL}}^{2D}(x, y) = V_0 [\cos^2(kx_a(t) + \theta_x) + \cos^2(ky_a(t) + \theta_y)], \quad (12)$$

where  $k$  and  $\theta_{x,y}$  are, respectively, the wavenumber and phase of the OL in the  $x$  and  $y$  direction. Here we observe that each 2D minimum (or maximum) is no longer isolated, and that between two minima (or maxima) there are areas for which the vortex can escape (near the saddle points of the potential). This is exactly what we observed when attempting to drag a vortex using the 2D OL (12) without sufficient adiabaticity. The vortex would meander around the various facets of the lattice outside of our control. To overcome this one needs to displace the potential with a high degree of adiabaticity. In doing so, we were successful in dragging the vortices under some restraints (relatively small displacements from the trap center). An example of a partially successful vortex dragging by an OL with potential (12) is presented in Fig. 7. As it can be observed from the figure, the vortex (whose center is depicted by a “plus”) is dragged by the OL (whose center is depicted by a cross) for some time. However, before the OL reaches its final destination, the pinning is lost and the vortex jumps to the neighboring OL well to the right. This clearly shows that vortex dragging with an OL is a delicate issue due to the saddle points of the OL that allow the vortex to escape. Nonetheless, for sufficient adiabaticity, with a strong enough OL and for small displacements from the trap center, it is possible to successfully drag the vortex. A more detailed study of the parameters that allow for a successful dragging with the OL (i.e., relative strength and frequency of the lattice and adiabaticity) falls outside of the scope of the present manuscript and will be addressed in a future work.

## B. Vortex Capturing

A natural extension of the above results is to investigate whether it is possible to capture a vortex that is already precessing by an appropriately located and crafted impurity. This idea of capturing, paired with the dragging ability, suggests that a vortex created off-center, which is typically the case in an experimental setting, can be captured, pinned and dragged to a desired location either at the center of the trap or at some other distance off-center. We now give a few examples demonstrating that it is indeed possible for a localized impurity to capture a moving vortex. The simulation begins with a steady-state solution of a vortex pinned by an impurity at a prescribed radius and a second impurity on the opposite side of the trap at a different radius. Initial numerical experiments have been done to determine the importance of the difference in these distances from the trap center.

As is shown in Fig. 8 the capturing impurity must be located sufficiently lower (i.e., closer to the trap center)

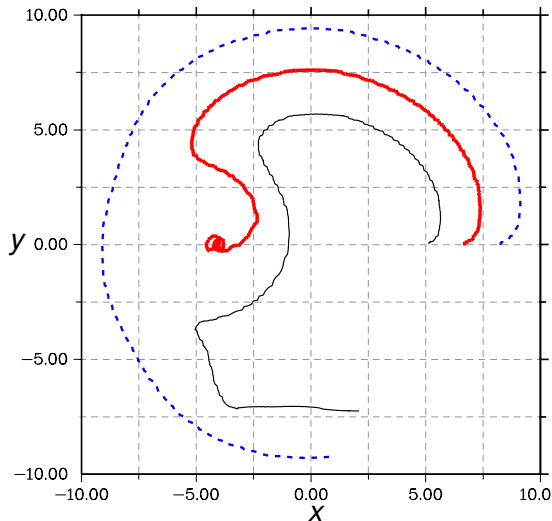


FIG. 8: (Color online) Capturing a precessing vortex by a stationary impurity. The different paths correspond to isolated vortices that are released by adiabatically turning off a pinning impurity at the following off-center locations: (5,0) (thin black line), (6.5,0) (thick red line) and (8,0) (blue dashed line). The capturing impurity is located at (-4,0). The first and third cases fail to produce capturing while the second case manages to capture the vortex. One interesting feature that we observed in the case of successful capture is that, before it gets captured, the vortex gets drawn into the impurity potential, but then almost gets knocked back out by the phonon radiation waves created from the capture which bounce around within the condensate.

than the trapping impurity in order for the vortex to be pulled from its precession and be captured by the impurity. Intuitively one might come to the conclusion that if the vortex and impurity were located the same distance away from the center of the trap, then the vortex should be captured. But due to the interaction between the vortex and the impurity that was discussed earlier, as the vortex approaches the impurity, it begins to interact with it by precessing clockwise around the impurity. Thus the orientation of the vortex and impurity with respect to the trap center greatly determines the dynamics. This combination of the interactions of the vortex with the trap and the vortex with the impurity then dictates that for a vortex to be captured by the impurity while precessing around the harmonic trap and rotating around the impurity, the impurity must be positioned at least closer to the trap center than the initial distance between the vortex and the trap center.

## V. CONCLUSIONS

In summary, we studied the effects on isolated vortices of a localized impurity generated by a narrowly focused laser beam inside a parabolic potential in the context of Bose-Einstein condensates (BECs). We not only exam-

ined the dynamics (dragging and capture) of the vortex solutions in this setting, but also analyzed in detail the stationary (pinned vortex) states, their linear stability and the underlying bifurcation structure of the problem.

As is already well known, the harmonic trap is responsible for the precession of the vortex around the condensed cloud. We have further demonstrated that a narrowly focused blue-detuned laser beam induces a local attractive potential that is able to pin the vortex at various positions within the BEC, and we investigated the dependence of pinning as a function of the laser beam parameters (width and power) for different locations in the condensed cloud. For a fixed beam width, we then explored the underlying bifurcation structure of the stationary solutions in the parameter space of pinning position and beam power. We found that for sufficiently high beam intensity it is possible to overcome the vortex precession and to *stably* pin the vortex at a desired position inside the condensed cloud. We also studied the conditions for a vortex to be dragged by an adiabatically moving beam and concluded that for sufficiently high intensity beams and for sufficient adiabaticity it is possible to drag the vortex to almost any desired position within the BEC cloud. The possibility of vortex dragging using periodic, two-dimensional, optical lattices was also briefly investigated. Due to the lattice's saddle points between consecutive wells, the vortex is prone to escape to neighboring wells and, therefore, dragging with optical lattices is arguably less robust than its counterpart with focused laser beams. Finally, we presented the possibility of capturing a precessing vortex by a stationary laser beam. Due to the combined action of the precession about the harmonic trap and the precession about the localized impurity, the stationary laser must be carefully positioned to account for both precessions so that the vortex can be successfully captured by the laser beam.

This work paves the way for a considerable range of future studies on the topic of vortex-impurity interactions. Among the many interesting possibilities that can be considered, we mention the case of more complex initial conditions, such as higher topological charge ( $\pm s$ ) vortices, and that of complex dynamics induced by the effects of multiple laser beams. For example, in the latter setting, we might envision a situation in which a single vortex is localized to a region within a BEC by appropriate dynamical manipulation of multiple laser beams *without* relying on vortex pinning. Such additional studies may provide a more complete understanding of the physics of manipulating vortex arrays by optical lattices. Additional investigations will also need to consider the role of finite temperature and damping, as well as the consequences of moving impurities located near the Thomas-Fermi radius where density is low and critical velocities for vortex shedding are much lower than near the BEC center.

Another natural extension of our work is to study the manipulation of vortex lines in three-dimensional condensates. It would be interesting to test whether the

beam could stabilize a whole vortex line (suppression of the so-called Kelvin modes [34]) and, moreover, change the orientation of a vortex [35]. Along this vein, a more challenging problem would be to study the pinning and manipulation of vortex rings by laser sheets; see e.g. [36]. These settings would also present the possibility of identifying a richer and higher-dimensional bifurcation structure.

**Acknowledgements.** PGK gratefully acknowledges support from the NSF-CAREER program (NSF-DMS-0349023), from NSF-DMS-0806762 and from the Alexander von Humboldt Foundation. RCG gratefully acknowledges support from NSF-DMS-0806762.

- 
- [1] P.W. Anderson, Phys. Rev. Lett. **9**, 309 (1962); A.M. Campbell and J.E. Evetts, Advan. Phys. **21**, 199 (1972); O. Daldini, P. Martinoli, and J.L. Olsen, Phys. Rev. Lett. **32**, 218 (1974); L. Civale *et al.*, Phys. Rev. Lett. **67**, 648 (1991).
  - [2] M. Baert, V.V. Metlushko, R. Jonckheere, V.V. Moshchalkov, and Y. Bruynseraede, Phys. Rev. Lett. **74**, 3269 (1995); C. Reichhardt, C.J. Olson, R.T. Scalettar, and G.T. Zimányi, Phys. Rev. B **64**, 144509 (2001); A.N. Grigorenko *et al.*, Phys. Rev. Lett. **90**, 237001 (2003).
  - [3] J.W. Reijnders and R.A. Duine, Phys. Rev. Lett. **93**, 060401 (2004); H. Pu, L.O. Baksmaty, S. Yi, and N.P. Bigelow, Phys. Rev. Lett. **94**, 190401 (2005); J.W. Reijnders and R.A. Duine, Phys. Rev. A **71**, 063607 (2005).
  - [4] S. Tung, V. Schweikhard, and E.A. Cornell, Phys. Rev. Lett. **97**, 240402 (2006).
  - [5] Rajiv Bhat, L.D. Carr, and M.J. Holland, Phys. Rev. Lett. **96**, 060405 (2006); Daniel S. Goldbaum and Erich J. Mueller, Phys. Rev. A **77**, 033629 (2008).
  - [6] E.K. Dahl, E. Babaev, and A. Sudbø, Phys. Rev. Lett. **101**, 255301 (2008).
  - [7] R. Geurts, M.V. Milošević, and F.M. Peeters, Phys. Rev. A **78**, 053610 (2008).
  - [8] P.G. Kevrekidis, D.J. Frantzeskakis, and R. Carretero-González (eds). *Emergent Nonlinear Phenomena in Bose-Einstein Condensates: Theory and Experiment*. Springer Series on Atomic, Optical, and Plasma Physics, Vol. **45**, 2008.
  - [9] R. Carretero-González, D.J. Frantzeskakis and P.G. Kevrekidis. Nonlinearity, **21** R139 (2008).
  - [10] R. Carretero-González, P.G. Kevrekidis, D.J. Frantzeskakis, and B.A. Malomed. Proc. SPIE Int. Soc. Opt. Eng. **5930** (2005) 59300L.
  - [11] G. Herring, P.G. Kevrekidis, R. Carretero-González, B.A. Malomed, D.J. Frantzeskakis, and A.R. Bishop. Phys. Lett. A, **345** (2005) 144.
  - [12] P.G. Kevrekidis, D.J. Frantzeskakis, R. Carretero-González, B.A. Malomed, G. Herring, and A.R. Bishop. Phys. Rev. A, **71** (2005) 023614.
  - [13] M.A. Porter, P.G. Kevrekidis, R. Carretero-González, and D.J. Frantzeskakis. Phys. Lett. A, **352** (2006) 210.
  - [14] V.V. Konotop, V.M. Pérez-García, Y.-F. Tang and L. Vázquez, Phys. Lett. A **236**, 314 (1997).
  - [15] V.V. Konotop and V.E. Vekslerchik, Phys. Rev. E **49**, 2397 (1994).
  - [16] D.J. Frantzeskakis, G. Theocharis, F.K. Diakonou, P. Schmelcher, and Yu.S. Kivshar, Phys. Rev. A **66**, 053608 (2002).
  - [17] Yu.S. Kivshar and X. Yang, Phys. Rev. E **49**, 1657 (1994).
  - [18] G. Theocharis, D.J. Frantzeskakis, R. Carretero-González, P.G. Kevrekidis and B.A. Malomed. Math. Comput. Simulat. **69** (2005) 537.
  - [19] P.G. Kevrekidis, R. Carretero-González, G. Theocharis, D.J. Frantzeskakis and B.A. Malomed. Phys. Rev. A, **68** 035602 (2003).
  - [20] G. Theocharis, D.J. Frantzeskakis, R. Carretero-González, P.G. Kevrekidis, and B.A. Malomed. Phys. Rev. E, **71** (2005) 017602.
  - [21] E.P. Gross. *Nuovo Cim.*, **20** (1961) 454.
  - [22] L.P. Pitaevskii. *Sov. Phys. JETP*, **13** (1961) 451.
  - [23] A.L. Fetter, J. Low Temp. Phys. **113**, 189 (1998).
  - [24] A.A. Svidzinsky and A.L. Fetter, Phys. Rev. Lett. **84**, 5919 (2000).
  - [25] E. Lundh and P. Ao, Phys. Rev. A **61**, 063612 (2000).
  - [26] J. Tempere and J.T. Devreese, Solid State Comm. **113**, 471 (2000).
  - [27] D.S. Rokhsar, Phys. Rev. Lett. **79**, 2164 (1997).
  - [28] S.A. McGee and M.J. Holland, Phys. Rev. A **63**, 043608 (2001).
  - [29] B.P. Anderson, P.C. Haljan, C.E. Wieman and E.A. Cornell, Phys. Rev. Lett. **85**, 2857 (2000).
  - [30] P.O. Fedichev and G.V. Shlyapnikov, Phys. Rev. A **60**, R1779 (1999).
  - [31] Y.S. Kivshar, J. Christou, V. Tikhonenko, B. Luther-Davies, and L.M. Pismen, Opt. Comm. **152**, 198 (1998).
  - [32] N.G. Parker, N.P. Proukakis, C.F. Barenghi, and C.S. Adams, Phys. Rev. Lett. **92**, (2004) 160403.
  - [33] B. Jackson, J.F. McCann, and C.S. Adams. Phys. Rev. Lett. **80**, 3903 (1998).
  - [34] V. Bretin, P. Rosenbusch, F. Chevy, G.V. Shlyapnikov, and J. Dalibard, Phys. Rev. Lett. **90**, 100403 (2003).
  - [35] P.C. Haljan, B.P. Anderson, I. Coddington, and E.A. Cornell, Phys. Rev. Lett. **86**, 2922 (2001).
  - [36] N.S. Ginsberg, J. Brand and L.V. Hau, Phys. Rev. Lett. **94**, 040403 (2005).